Theor Chem Account (2008) 121:43–52
DOI 10.1007/s00214-008-0444-5

REGULAR ARTICLE

A charge iteration-corrected extended-Hückel study of the electronic and spectroscopic properties of conjugated heterocycles

Charles M. Castevens, IV

Received: 21 January 2008 / Accepted: 24 March 2008 / Published online: 14 May 2008

Abstract A computationally inexpensive modified extended-Hückel method using coordinates from STO-6G(d,p) geometry optimizations is described and shown to accurately simulate the spectra of conjugated heterocycles. The origins of the natural optical activities of blue indophenines and diheptylindophenines, and several related brown, red, and colorless compounds, were investigated with this method to show how it can be used to examine the changes in spectra and electronic structure that occur with substituent additions and changes. Diheptylindophenines were found to be blue because of absorptions from electronic transitions between spatially congruent π and π^* molecular orbitals delocalized across carbon, nitrogen, oxygen, and sulfur atomic orbitals. The effects of conjugated thiophene moieties replacing the isatin moiety β-carbonyls move these absorptions to the blue relative to their locations in *n*-heptylisatin, and the diheptyl groups move these absorptions slightly to the red relative to indophenines.

Keywords CNDO-S/D · Extended-Hückel · Indophenine · MCD · SEA//STO-6G(d,p) · UV–visible

1 Introduction

Colored heterocycles have long been studied by chemists and physicists. As an example, in 1879 Adolph von Baeyer reported that red isatin mixed with benzole and sulphuric acid produces a dark blue compound, indophenine [1,2].[1] Victor Meyer later discovered thiophene while studying this reaction, and determined that the indophenine-producing reaction was between isatin and thiophene, an impurity in the benzole used, and not between isatin and benzene as first thought [3–6].[2] Several correct and incorrect structures for indophenine were proposed over the decades [7–10],[3] and from analysis of 2D ^{1}H NMR COSY spectra in 1993 Tormos et al. proposed that there are six stereoisomers of diheptylindophenine in solution [11], shown in Fig. 1 with their labels **8a–8f** (labeling from Tormos is used throughout). They also proposed these are the diheptyl analogues of indophenine (**i8a–i8f**), which would then have the formula $C_{24}H_{14}N_2O_2S_2$. In addition to a deep blue solution of **8a–8f** ($\lambda_{max} = 634$ nm in CH_2Cl_2), they isolated related colorless (**7**, **11**) and brown (**9a**, $\lambda_{max} = 526$ nm) molecules also containing isatin and thiophene moieties.

Electronic supplementary material The online version of this article (doi:10.1007/s00214-008-0444-5) contains supplementary material, which is available to authorized users.

C. M. Castevens, IV (✉)
USS Dwight D. Eisenhower (CVN 69),
AIMD, FPO AE 09532-2830, USA
e-mail: pen7cmc@ureach.com

[1] The formula of indophenine is given as $C_{20}H_{15}NO$.

[2] Ref. [6]: The formula of indophenine is given as $C_{12}H_7NOS$.

[3] Ref. [7]: a structure similar to that of **i8b** is given as the structure of indophenine, with the difference being that an α-carbonyl derivative of isatin is given, instead of the β-carbonyl derivative now known to be the correct structure. Ref. [8]: **i8b** is given as the structure of indophenine. Ref. [9] shows a structure consisting of four fused rings, NH, O, and S occupying one ring each, with a formula of $C_{12}H_7NOS$.

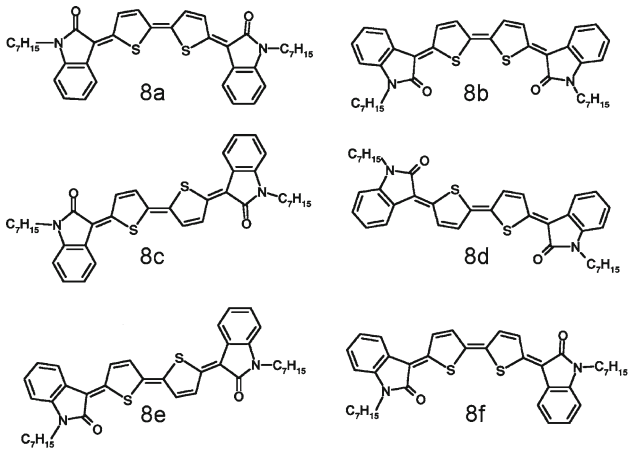

Fig. 1 The six stereoisomers of diheptylindophenine

2 Calculation details

Of course numerous other conjugated indole, isatin, pyrrole, and thiophene moiety molecules are currently being studied in the gas phase, and as building blocks of lasers, light emitting diodes, solar energy conversion devices, and polymers [12–26]. In addition to such applications, these and other heterocycles are interesting subjects for theoretical studies as they have many low-energy electronic transitions: N, O, and S-containing chromophores with $\pi^* \leftarrow$ n and $\pi^* \leftarrow \pi$ transitions, and $\pi^* \leftarrow \pi$ transitions in the molecular orbitals (MOs) with large carbon 2p atomic orbital (AO) contributions. The 90^o $\pi^* \leftarrow$ n transitions will have weak absorptions in the UV–vis region from symmetry considerations, but can have strong magnetic circular dichroism (MCD) transition moments as the MCD B term (the magnetic rotational strength) uses a product of electric and magnetic transition moments between the ground state and multiple excited states [27,28].

The aim of this research was to find a way to model the UV–vis spectra of large conjugated molecules, without creating yet another new (and ever more computationally expensive) method. The objective was not to expend great computational effort to find the lowest calculated energies of these molecules, or accurately describe higher-lying excited states, as only the origins of low energy transitions in the visible region were being examined. This means that large basis sets such as the modified aug-cc-pVTZ basis with additional diffuse Rydberg functions that have been used to model thiophene [29] were not a prerequisite.

MCD calculations with coordinates from STO-6G(d,p)[4] geometry optimizations have been used to examine indole moiety molecules before [32], and, as shown below, good agreement with experimental UV–vis spectra of simple thiophene and indole moiety molecules were obtained with the same coordinates input to an extended-Hückel UV–vis spectra-simulating program previously used to study small metal and metal-containing clusters. Also, STO-6G(d,p) bond lengths for isatin were within 0.01 Å of those in the crystal structure [23]. Therefore, ground-state (S_0) structures of molecules were optimized by taking the initial atomic coordinates created by Sybyl [33] and geometry optimizing them at the STO-6G(d,p) level with GAMESS [34,35] until the RMS gradients were 10^{-6} hartree/bohr or lower, unless otherwise noted.

MCD spectra were simulated with a program that performs semi-empirical CNDO/S-D (complete neglect of differential overlap/spectroscopic-deorthogonalized) CI-S (configuration interaction, singles only) calculations using Slater-type orbitals [32,36–38]. The usual 0.585 scaling factor was used to adjust for the overestimation of excitation energies by this method [39], and parameters for sulfur were taken from Ref. [40]. Ninety-nine configurations were used, HOMO to LUMO, LUMO+1, …, LUMO+13, then HOMO-1 to LUMO, LUMO+1, …, LUMO+12, then HOMO-2 to LUMO, LUMO+1, …, LUMO+11, and so on until 99 configurations were chosen. The results from this program were checked for accuracy by comparing its output against the published output of another program [41].

To compare several computationally inexpensive UV–vis spectra simulating methods, absorption spectra were calculated using ZINDO/S both with and without the random-phase approximation (RPA/ZINDO/S) in ArgusLab 4.0.1 [42] and Gaussian 98 [43], the CI-S method using small basis sets in GAMESS, and the self-consistent charge (SSC) iteration-corrected [44] extended-Hückel molecular orbital (EHMO) atom superposition and electron delocalization (AESD) method [45] (the SEA method) used for this article.

The ICON-EDiT program calculates molecular properties using a weighted, distance-dependent Wolfsburg–Helmholtz formula as part of the SEA method. The only non-default values set were to use charge iteration, which was performed on all atoms, with each atom being treated individually. Detailed descriptions of the SEA method and ICON-EDiT program can be found in Refs. [44–50], and a brief overview that closely follows those references follows.

2.1 Implementation of the SEA extended-Hückel method

The problem is to solve an approximation of the n-electron Schrödinger's equation $H\Psi = \mathrm{E}\Psi$ within the usual Hartree–Fock and Born–Oppenheimer approximations. Viewing this as a matrix equation it can be rearranged as $(H - EI)\Psi = 0$,

[4] STO-6G(d,p) is also known as STO-6G**. D and p polarization exponents (0.65 on sulfur and 1.1 on hydrogen) used by GAMESS [34] for STO-6G(d,p) are from the 6-31G(d) and 6-31G(d,p) values of Refs. [30,31]. GAMESS does not add d exponents to H through F when using STO-6G(d,p).

with I being the identity matrix, to solve for an eigenvalue E.

As is the case for other linear combination of atomic orbitals-molecular orbital approaches, the wave function Ψ is expanded as the sum of atomic orbitals χ with coefficients c,

$$\Psi = \sum_{\mu=1}^{n} c_\mu \chi_\mu \tag{1}$$

with χ chosen to be Slater-type orbitals centered on each atom, labeled by μ and numbered from 1 to n.

H is a modified Hückel matrix. Because charge iteration-correction was used, the diagonal Hückel matrix elements H_{ii} were equal to −VSIE(Q), the opposite of the valence state ionization energy (VSIE) of orbital i when the atom has a total charge Q. VSIE(Q) is equal to AQ^2+BQ+C, with A, B, and C being empirically determined energies. Using hydrogen as an example, A for the 1s VSIE($1s^1$) is 13.61853 eV.

The off-diagonal Coulomb integrals H_{ij} were calculated using $H_{ij} = KS_{ij}\ (H_{ii} + H_{jj})/2$, with S_{ij} representing the overlap matrix $\langle\chi_i|\chi_j\rangle$, and K representing the distance-dependent Wolfsberg–Helmholtz parameter

$$K = 1 + k\left(\frac{\exp(-\delta(R-d_0))}{1+([(R-d_0)-|R-d_0|]\cdot\delta^2)}\right) \tag{2}$$

where $\delta = 0.35\,\text{Å}^{-1}$, d_0 is the sum of the ith and jth atomic orbital radii, R is the distance between atoms, and $k = \kappa + \Delta^2 - \Delta^4\kappa$, with $\Delta = (H_{ii} - H_{jj})/(H_{ii} + H_{jj})$ and $\kappa = 1$. These are the default values used in ICON-EDiT.

With these and other approximations, we are left with the eigenvalue equation $(H - ES)\cdot c = 0$ to solve. Transition energies were calculated by taking the differences in the eigenvalues between occupied and unoccupied orbitals.

2.2 Implementation of the SEA extended-Hückel method: oscillator strengths

The dimensionless oscillator strength f can be computed from the dipole length. The electronic transition dipole moment $\boldsymbol{\mu}^{\text{ed}}_{nm}$ between wave functions ψ_n and ψ_m is defined as

$$\boldsymbol{\mu}^{\text{ed}}_{nm} = \left\langle \psi_n \left| \boldsymbol{\mu}^{\text{ed}} \right| \psi_m \right\rangle \tag{3}$$

$$\boldsymbol{\mu}^{\text{ed}} = -\left(\sum_i e\mathbf{r}_\mathbf{j}\right). \tag{4}$$

Using the relationship between the oscillator strength of the transition between n and m, f_{nm}, and the dipole moment,

$$f_{nm} = \frac{8\pi^2 c m_e \boldsymbol{\nu}\left|\boldsymbol{\mu}^{\text{ed}}_{nm}\right|^2}{3he^2} \tag{5}$$

and the definition of the transition dipole length D_{nm}

$$|D_{nm}|^2 = \frac{\left|\boldsymbol{\mu}^{\text{ed}}_{nm}\right|^2}{e^2} \tag{6}$$

leads us to

$$f_{nm} = I_0 \boldsymbol{\nu} |D_{nm}|^2 \tag{7}$$

with I_0 equal to 1.085×10^{-5} cm/Å^2, $\boldsymbol{\nu}$ is the wave number of the transition in cm^{-1}, c is the speed of light in a vacuum, m_e is the mass of an electron, h is Planck's constant, and e is the charge of the electron.

Using Eqs. 1, 3, 4 and 6, D_{nm} can be rewritten as

$$D_{nm} = \langle\psi_n\,|\mathbf{r}|\,\psi_m\rangle = \sum_{ks} c_k^n c_s^m\,\langle\chi_n\,|\mathbf{r}|\,\chi_m\rangle. \tag{8}$$

As the AOs and coefficients are calculated as part of the extended-Hückel method, once these are known the oscillator strengths f_{nm} can be found for each transition using equations 7 and 8 [45,50].

3 Results

The ability of SEA//STO-6G(d,p) to model UV–vis spectra will be demonstrated primarily by examining diheptylindophenine and its constituent moieties. Consider building a diheptylindophenine molecule in this way: start with pyrrole, and expand the pyrrole to indole (2,3-benzopyrrole), then isatin (1H-indole-2,3-dione), n-propylisatin (**5**, 1-propyl-indole-2,3-dione), and n-heptylisatin (**6**, 1-hepyl-indole-2,3-dione). Add a thiophene moiety (and an –OH group) to form 1-heptyl-3-hydroxy-3-thienyl-2-indolinone (**11**), and then remove the –OH while adding another conjugated n-heptylisatin to form **9a**. Finally, replace the single thiophene moiety in **9a** with two thiophene moieties to form diheptylindophenines **8a–8f**.

Basic results from the smaller molecules and the changes in spectra caused by each addition while going from thiophene and pyrrole to **8a–8f** will be shown first, in addition to results from a few other large conjugated molecules. Then, the origins of the natural optical activities of **8a–8f** will be examined in detail.

Thiophene (C_{2v}): The strong absorption band observed experimentally at 215 nm [12], that is calculated by symmetry-adapted cluster-configuration interaction (SAC-CI) [29] and multi-reference configuration interaction calculations [51] to consist of two $\pi^* \leftarrow \pi$ transitions, was calculated to consist of two $\pi^* \leftarrow \pi$ transitions at 213.45 nm ($f = 0.43430$) and 210.46 nm ($f = 0.61904$). The ArgusLab (AL) ZINDO/S value was 257.0 nm, and AL RPA/ZINDO/S at 276.94 nm, both well to the red.

Pyrrole (C_{2v}): The $^1B_2$ transition measured at 217 nm (5.7 eV) and calculated by the SAC/SAC-CI method to be

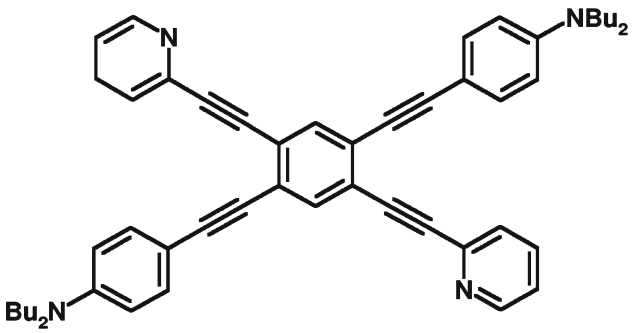

Fig. 2 Cruciform **3**

a $\pi^* \leftarrow \pi$ transition at 214 nm (5.80 eV) [21] was calculated here at 210.09 nm (5.90 eV, $f = 0.37589$). The Gaussian 98 (G98) ZINDO/S value was 242.89 nm, with AL ZINDO/S at 244.4 nm, and AL RPA/ZINDO/S 261.72 nm, all well to the red of the experimental value.

5,10,15,20-tetrakis(*N*-methylpyridinium-4-yl)-21H,23H-porphyrin ($TMPyP^{4+}$, D_2, RMS gradient = 8×10^{-6}): A porphyrin was chosen as a test case of a large, conjugated system with pyrrole moieties. $TMPyP^{4+}$ is water-soluble tetracationic porphyrin with a Soret band absorption at 422 nm [52,53]; this was calculated at 424.88 nm, with the absorptions in the visible from transitions between two occupied and two unoccupied orbitals [54–56].

Cruciforms: Dialkylamino- and pyridine-containing cruciforms, one of which is shown in Fig. 2 (C_i, RMS gradient $= 1.45 \times 10^{-5}$), have recently been characterized by several groups [57–59]. Haley′s cruciform **3** [57] has HOMO localized on the dibutylamino groups, and LUMO is localized on the pyridine rings. Cruciform **3** has absorption bands, in a solution of toluene, at 437 (broad), 380, 348, 339 and 285 nm, with 40–65 nm solvatochromism effects found in different solutions.[5] These were calculated at 419 (overlapping 428.06 and 417.03), 364.29, 336 (overlapping 345.13 and 331.65), 311.50, and 295 (overlapping 297.41, 294.05 and 291.00) nm in the gas phase, an average absolute error of less than 5%. The strong absorption at 428.06 nm is from a LUMO-2 ← HOMO transition between the donor *N*, *N*-dibutylaniline moieties and the acceptor pyridine moieties.

Blue Fluorescent Protein (BFP, *cis*-HSD, C_s): The gas phase and protein matrix spectra of several structures of BFP have been studied with TDDFT using B3LYP/6-31++G(d,p) (gas phase) and QM/MM (matrix) coordinates [60]. The *cis*-HSD configuration has an experimental λ_{max} in the matrix at 386 nm (3.21 eV), with shoulders at 369 nm (3.36 eV) and 406 nm (3.05 eV). The 406 nm shoulder is half as intense as the 386 nm peak, and the 369 nm shoulder appears only in calculations on non-planar structures. With a planar C_s geometry the SEA//STO-6G(d,p) values for the 386 and 406 nm absorptions are 366.35 nm (3.38 eV, $f = 0.29959$) and 406.67 nm (3.05 eV, $f = 0.15580$), respectively, and the TDDFT values were 324.67 nm (3.82 eV) and 382.67 nm (3.24 eV).

Indole (C_s): The $\pi^* \leftarrow \pi$ transition at 287 nm [61] was calculated at 287.13 nm ($f = 0.42676$).

Isatin (C_s): The lowest energy absorption in the visible was calculated to be a LUMO ← HOMO+3, $\pi^* \leftarrow \pi$ transition at 418.85 nm ($f = 0.35975$) on the carbonyl group. Experimentally, a broad peak is centered near 420 nm [61]. One other absorption in the visible was calculated at 608.30 nm ($f = 0.13052$), from an OC π^* ← NOC π transition. The absorption in isatin corresponding to the 287 nm indole absorption blue-shifted to 273.79 nm ($f = 0.59883$), which, along with a CNO π^* ← OC π calculated to occur at 279.91 nm ($f = 0.16508$), are seen experimentally as another broad peak near 296 nm.

The nomenclature "OC π^* ← NOC π" will be used to indicate the largest AO coefficients on the π^* MO were from oxygen and carbon AOs, and from nitrogen, oxygen and carbon AOs for the π MO. Multiple atom types listed together (e.g., NOC) indicate the AO coefficients from all those atoms were above ‖0.2‖, these AO coefficients usually ranging from ‖0.2‖ to ‖0.4‖, with the atoms listed in order of largest to smallest AO contributions. As all the MOs have multiple C AO coefficients in the ‖0.2‖–‖0.3‖ range, *C* will not be listed unless its AO coefficients are greater than the N, O, and/or S coefficients, or has coefficients greater than ‖0.3‖, or are the only coefficients greater than ‖0.2‖.

5 (*n*-propylisatin, C_s): The strongest absorption in the visible was calculated to be from a LUMO ← HOMO+3, OC π^* ← CO π transition at 414.64 nm ($f = 0.376306$). One other strong absorption in the visible was calculated at 671.41 nm ($f = 0.120573$), from a LUMO ← HOMO+1, OC π^* ← NOC π transition. The absorption in *n*-propylisatin corresponding to the 273.79 nm isatin absorption blue-shifted to 257.50 nm ($f = 0.585790$).

6 (*n*-heptylisatin, C_s): Absorptions in the visible were calculated at 414.63 nm ($f = 0.37633$), 580.89 nm ($f = 0.00001$) and 671.77 nm ($f = 0.12051$). Transitions originating in the carbonyls of isatin, *n*-propylisatin, and *n*-heptylisatin are only minimally affected by the presence of an alkyl arm on the N, with a strong carbonyl transition for all three molecules remaining near 415 nm (418.85, 414.64, and 414.63 nm for these three molecules) regardless of alkyl arm presence or length. The weak 580.89 nm absorption is from a 90° C π^* ← O n transition. The 671.77 nm absorption is from a LUMO ← HOMO+1, OC π^* ← NOC π transition. The presence of an arm substantially red-shifts this absorption, from a calculated 608.30 nm in isatin, to 671.41 nm in *n*-propylisatin and 671.77 nm in *n*-heptylisatin.

7 (C_s): One of the stereoisomers of this colorless compound (Fig. 3) was examined and found to have no absorptions

[5] Haley, MM, Spitler, EL. Private communications, 8 February 2007.

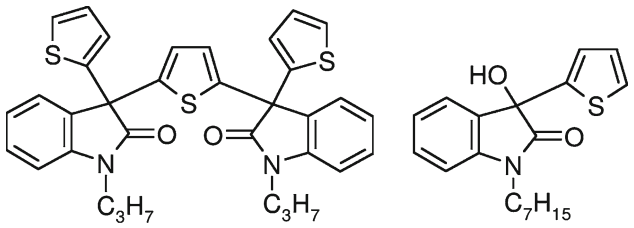

Fig. 3 Structures of **7** (left) and **11** (right)

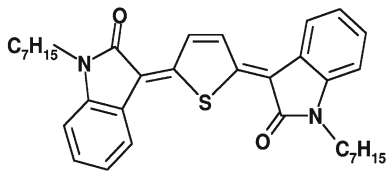

Fig. 4 Structure of **9a**

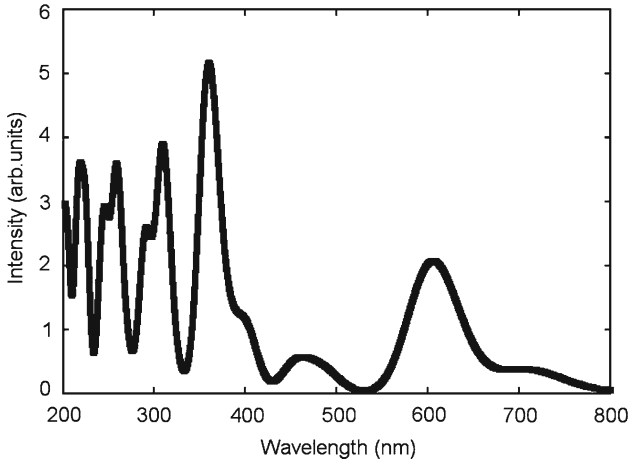

Fig. 5 Calculated UV–vis absorption spectrum of **8a–8f**

calculated in the visible. The closest absorption to the visible was at 391.44 nm ($f = 0.00051$), a carbonyl LUMO ← HOMO, OC π^* ← O n transition.

11 (1-heptyl-3-hydroxy-3-thienyl-2-indolinone, C_1): A weak carbonyl LUMO ← HOMO, OC π^* ← O n transition at 435.62 nm ($f = 0.00669$) was the only absorption calculated in the visible for this colorless compound. The next absorption, at 359.49 nm ($f = 0.50599$), is from a LUMO ← HOMO+1, OC π^* ← NO π transition. G98 ZINDO/S calculated the lowest-energy absorption at 332.74 nm ($f = 0.0051$), with the strongest absorption above 250 nm at 271.52 nm ($f = 0.2413$). AL ZINDO/S calculated similar values, 333.0 nm ($f = 0.005284$) and 274.8 nm ($f = 0.242770$), with RPA/ZINDO/S values of 334.4 and 295.7 nm.

9a (C_s): Only one isomer of **9** was isolated, **9a** (Fig. 4), with an experimentally measured λ_{max} of 526 nm in CH_2Cl_2, corresponding to the gas phase SEA//STO-6G(d,p) absorption found at 538.82 nm ($f = 0.53502$). Two weak absorptions were also calculated to lie the visible, at 665.34 nm ($f = 0.00957$, OC π^* ← NO π) and 426.11 nm ($f = 0.00030$, OC π^* ← O n).

The strong 538.82 nm absorption is from a LUMO ← HOMO+4, OC π^* ← NSC π transition. HOMO+4 has large 2p AO coefficients from S and both nitrogens, and LUMO's largest coefficients are from 2p AOs on both oxygens, all the thiophene moiety carbons, and isatin 3-position carbons (‖0.3034‖–‖0.3367‖). The weak 665.34 nm absorption is a LUMO ← HOMO+3, OC π^* ← NO π transition. The carbonyl absorptions found in *n*-propylisatin and *n*-heptylisatin near 415 nm, and in **11** at 436 nm, are at 426.11 and 428.95 nm in **9a**. These two non-degenerate absorptions are due to the dissimilar environments of the two oxygens, with the 428.95 nm transition from the O *syn* to the S having a zero calculated oscillator strength.

The 526 nm absorption was calculated by G98 ZINDO/S, CI-S/STO-6G(d,p), CI-S/6-31+G(d,p)//RHF/STO-6G(d,p), and RPA/STO-6G(d,p) to occur at 403.78, 266.33, 327.67, and 283.10 nm, all substantially below the experimental value.

8a–8f: A solution of **8a–8f** in CH_2Cl_2 has an experimentally measured λ_{max} at 634 nm, with each stereoisomer having gas phase SEA//STO-6G(d,p) λ_{max} values at 453.89, 607.39, 602.37, 611.36, 606.94, and 603.03 nm, respectively. **8a** has a second strong absorption at 598.55 nm of the same origin as absorptions near 606 nm in **8b–8f**. A simulated spectrum consisting of the sum of all the calculated gas phase spectra in the region measured experimentally, 200–800 nm,[6] weighted according to their relative concentration in solution and using gaussians with half-widths of 750 cm^{-1}, is shown in Fig. 5. The most intense calculated gas phase absorption in the visible is at 606 nm, less than a 4.5% error to the blue of the experimental value in solution. Other absorptions, observed experimentally at 391 nm (sh), 339 nm (sh), and 248 nm, were calculated at 360 nm (O π^* ← N π, shoulder O π^* ← CS π 395 nm), 309 nm (overlapping CO π^* ← N π and C π^* ← N π, shoulder O π^* ← N π 291 nm), and 258 nm (C π^* ← C π). One strong absorption was found in the IR, from overlapping 1,015–1,033 nm absorptions, and is from LUMO ← HOMO+2, O π^* ← O π transitions.

Transitions in the visible with oscillator strengths greater than 1×10^{-5} are listed in Table 1, and are summarized below and in the electronic supplementary material.

8a (C_{2v}): The strong 453.89 nm absorption is from OC π^* ← SCN π transitions between MOs spanning the isatin and thiophene moieties. The 598.55 nm absorption is from a LUMO ← HOMO+4, OC π^* ← NCO π transition.

[6] Cava, MP. Private communication, 5 June 2003.

Table 1 Molecular orbital types, wavelengths in nm, and oscillator strengths (in paranthesis) of transitions with oscillator strengths greater than 1×10^{-5} in the visible for **8a–8f** (w = weak oscillator strength of 3×10^{-4} or less)

Type	**8a** (C_{2v})	**8b** (C_{2v})	**8c** (C_{2h})	**8d** (C_{2h})	**8e** (C_s)	**8f** (C_s)
$\pi^* \leftarrow \pi$	400.98 (0.01)	400.59 (0.18)	400.99 (0.17)	400.77 (0.29)	400.85 (0.07)	400.72 (0.20)
$\pi^* \leftarrow \pi$			441.56 (w)	444.21 (w)	443.03 (w)	
$\pi^* \leftarrow \pi$	440.49 (w)	443.48 (w)			443.58 (w)	442.15 (w)
$\pi^* \leftarrow \pi$	453.89 (0.26)	458.53 (0.03)			456.43 (0.03)	456.23 (0.12)
$\pi^* \leftarrow \pi$	483.72 (0.02)	484.19 (0.18)			485.89 (0.10)	483.91 (0.04)
$\pi^* \leftarrow$ n	493.12 (w)	496.11 (w)			494.71 (w)	494.95 (w)
$\pi^* \leftarrow$ n			494.56 (w)		497.09 (w)	496.33 (w)
$\pi^* \leftarrow \pi$	598.55 (0.20)	607.39 (0.42)	602.37 (0.29)	611.36 (0.42)	606.94 (0.29)	603.03 (0.36)
$\pi^* \leftarrow \pi$	708.37 (0.01)	709.52 (0.20)			712.25 (0.09)	708.97 (0.05)

8b (C_{2v}): The strongest absorption, at 607.39 nm, is from a LUMO ← HOMO+4, OC π^* ← NCO π transition, which occurs at 598.55 nm in **8a**. In **8a** and **8b**, the AO coefficients for S in HOMO+4 are between ‖0.195‖ and ‖0.199‖, just below the ‖0.2‖ cut-off for listing as part of the MO.

8c and **8d** (C_{2h}): The strongest absorptions, at 602.37 and 611.36 nm, respectively, are from LUMO ← HOMO+4, OC π^* ← NOCS π transitions, comparable to the 607.39 nm absorption in **8b**. The strong absorptions near 400 nm (**8c** $f = 0.17164$, **8d** $f = 0.29357$) are from OS π^* ← N π transitions.

8e and **8f** (C_{2s}): The strongest absorptions, at 606.94 and 603.03 nm, respectively, are HOMO+4 ← LUMO, OC π^* ← NOCS π transitions.

G98's ZINDO/S calculated λ_{max} values for **8a–8d** at 429.84, 438.64, 429.13, 436.23, 433.04, and 434.57 nm, with oscillator strengths ranging from 1.7008 (**8a**) to 1.8783 (**8d**). HOMO to LUMO transitions with coefficients of ≈ 0.66 dominated these lowest energy excitations. AL ZINDO/S calculated λ_{max} at 414.1 421.6, 413.3, 419.0, 416.5, and 418.2 nm, with oscillator strengths ranging from 1.899642 (**8d**) to 1.729759 (**8f**). The 88 highest and 88 lowest MOs were used, vice the 104 with G98, due to memory limitations. The G98 ±88 MO values ranged from 417.96 (**8c**) to 427.13 (**8a**) nm. RPA/STO-6G(d,p) calculations with 10 excited states produced lowest transition energies from 320.84 (**8a**) to 331.15 (**8c**) nm, with oscillator strengths from 2.6357 (**8f**) to 2.7988 (**8e**). A larger RPA/6-31+G(d)//RHF/STO-6G(d,p) calculation using 10 states, with **8d** as a test case, had a lowest non-zero absorption at 219.11 nm ($f = 0.0132$).

To summarize, the most accurate ZINDO/S calculations computed λ_{max} values 200 nm to far into the blue. Small RPA/STO-6G(d,p) calculations had even larger errors, over 300 nm to the blue. Gas phase SEA//STO-6G(d,p) values were less than 30 nm to the blue, usually ranging from 3 to 5% below the experimentally measured values in solution.

i8a–i8f, the N–H indophenine analogues of the N–C_7H_{15} diheptylindophenines, have gas phase SEA//STO-6G(d,p) λ_{max} values in the visible at 447.11, 564.88, 559.85, 568.12, 564.08, and 560.88 nm, respectively. **i8a** has a second strong absorption at 556.79 nm of the same origin as the absorptions near 563 nm in **i8b–i8f**. The origins of these absorptions are the same as, and are shifted to the blue relative to, the **8a–8f** diheptylindophenines, consistent with the blue shift seen from *n*-heptylisatin to isatin. The simulated spectrum using gaussians with half-widths of 750 cm^{-1} has a calculated λ_{max} at 563 nm, a 2.4% error to the red of the 550 nm seen experimentally [62,63]. The overlapping O π^* ← O π absorptions near 1,020 nm in **8a–8f** are calculated near 1,020 nm in **i8a–i8f** as well. G98 ZINDO/S calculated λ_{max} values in the visible region about 130 nm to the blue, at 427.33, 436.13, 426.61, 433.81, 430.57, and 431.10 nm, with oscillator strengths ranging from 1.6813 (**i8a**) to 1.8835 (**i8d**). The lowest energy CI-S/6-31+G(p) absorption, using **i8c** as a test case, was at 360.43 nm ($f = 2.727968$), from a HOMO ← LUMO, C π^* ← CS π transition.

4 Discussion

Diheptylindophenines and indophenines **8a–8f** and **i8a–i8f** are blue because of absorptions that arise from $\pi^* \leftarrow \pi$ transitions between spatially congruent MOs delocalized across the conjugated isatin and thiophene moieties. These transitions, calculated to occur in the gas phase from 598.55 to 611.36 nm in **8a–8f**, are seen experimentally in a solution of all six stereoisomers in CH_2Cl_2 at 634 nm. The orientation of the thiophene moiety relative to the isatin moiety has little effect on the calculated λ_{max} of each individual indophenine, varying it about 2%, but orientation does change the calculated oscillator strength for this transition by over a factor of two.

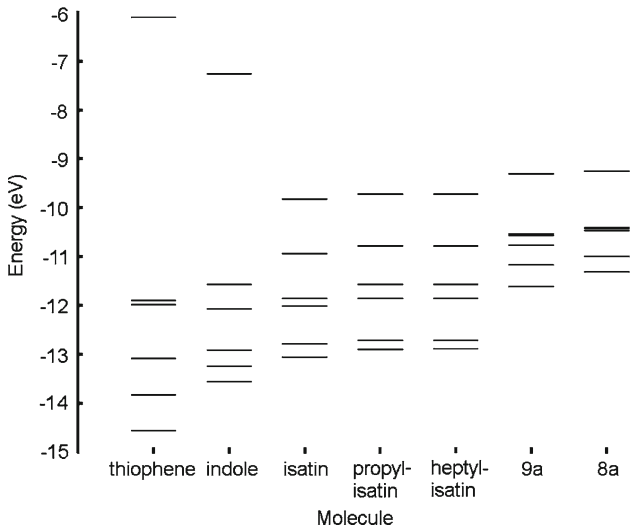

Fig. 6 Calculated energy levels for LUMOs and five highest occupied molecular orbitals

The strongest visible region absorptions in **8a–8f** can be divided into three regions: near 400, 450–500, and 605–710 nm. The first region has a single absorption near 400 nm from an OS $\pi^* \leftarrow$ N π transition. The second region has absorptions from O $\pi^* \leftarrow$ OC π transitions, with the π MOs spanning the oxygens and thiophene moieties, and a varying number of strong absorptions controlled by symmetry selection rules of the different isomers. The third region has two OC $\pi^* \leftarrow$ NOCS (or NCO) π transitions, one near 605 nm and the other near 710 nm. The 605 nm region absorption is the stronger of the 605 nm region and 710 nm region absorptions, by at least a factor of two.

Adding a propyl group to isatin to form *n*-propylisatin shifts the lower energy NOC π HOMO+1 orbital up 0.3 eV, and the higher energy OC π^* LUMO up by 0.1 eV, as shown in Fig. 6. This narrows the energy gap by 0.2 eV, resulting in a red shift of the OC $\pi^* \leftarrow$ NOC π absorption from 608 to 671 nm. A heptyl group instead of a propyl group shifts the energies of these two orbitals to within 0.01 eV of the propyl-shifted energies, resulting in a red-shift for *n*-heptylisatin to a similar wavelength, 672 nm. However, isatin, *n*-propylisatin and *n*-heptylisatin are reddish orange because each has a single absorption near 420 nm from an OC $\pi^* \leftarrow$ CO π transition, with a wavelength little changed regardless of the presence or absence of an alkyl arm on the nitrogen.

9a is brown because its LUMO is pushed up in energy by 0.41 eV relative to **6**'s LUMO by conjugation with a thiophene moiety and another *n*-heptylisatin, while the NS π HOMO+4 is lower in energy by 0.05 eV than **6**'s NOC HOMO+1. This moves λ_{max} for **9a** (LUMO $\leftarrow$ HOMO+4) to the red of **6** (LUMO $\leftarrow$ HOMO+1). **9a**'s N π HOMO+3 is similar to **6**'s N π HOMO+1, and is involved in the low-intensity 665.34 nm absorption.

Moving from **9a** to **8a–8f** by adding another conjugated thiophene moiety pushes HOMO+4 up another ≈0.31 eV, and LUMO up ≈0.06 eV, both shifts varying in the last digit depending on the particular diheptylindophenine. This narrows the gap by ≈0.25 eV relative to **9a**, resulting in a calculated red-shift from 539 nm in **9a** (LUMO $\leftarrow$ HOMO+4) to an average of 606 nm in **8a–8f** (LUMO $\leftarrow$ HOMO+4).

Replacing the N, O, and S atoms is predicted to shift all the absorptions instead of only strongly shifting one or a small number of them, with calculated absorptions for several test molecules shown in the electronic supplementary material. The MOs near HOMO and LUMO are not spatially separated, overlapping on the α-carbonyl groups, isatin 3-carbons, and thiophene moieties. Therefore, indophenines are functional chromophores, not functionalized chromophores such as cruciforms which have spatially separated donor (HOMO) and acceptor (LUMO) groups that can be chemically modified separately.

5 CNDO/S-D//STO-6G(d,p) MCD calculations

Tryptophan is the only amino acid with a strong positive (+) MCD absorption near 290 nm. This absorption originates from a N π–C π^* transition on the indole moiety, with indole itself having its strongest absorption at (+)280 nm, and isatin at (+)425(broad) [61]. Here the MCD transitions are described as occupied MO–unoccupied MO, in keeping with the notation used by the references in this section. Thiophene also has a strong π–π^* absorption, at (+)236 nm [13,14]. Tables of calculated MCD absorptions for **8a–8f** and **i8a–i8f** are in the electronic supplementary material, and are summarized here and in Table 2. In **8a–8f** and **i8a–i8f**, the lowest energy transitions were all CSO π–CO π^*, HOMO to LUMO transitions near (+)430 nm. These transitions also had the largest calculated oscillator strengths. As HOMO and LUMO are delocalized primarily across the thiophene moieties and the isatin carbonyl, the strongest MCD absorptions in indophenines are predicted to not be from N π–C π^* transitions that many indole moiety molecules have as the origins of their strongest absorptions, but from transitions that are similar to isatin's carbonyl-centered transitions seen as an absorption at (+)425 nm.

6 Conclusions

The SEA//STO-6G(d,p) method–UV–vis spectra calculations using a self-consistent charge iteration-corrected extended-Hückel method with coordinates from STO-6G(d,p) geometry optimizations–accurately simulates the spectra of colored and colorless heterocycles, usually calculating gas phase values slightly to the blue of those found in solution.

Table 2 CNDO/S-D calculated lowest and second-lowest energy MCD transitions

Molecule	Lowest			Second lowest		
	nm	Dip. len.	Origin	nm	Dip. len.	Origin
8a (C_{2v})	(+)427.33	1.57021	CSO π–CO π^*	(+)415.05	0.00060	CSO π–SC π^*
8b (C_{2v})	(+)438.05	1.60278	CSO π–CO π^*	(+)404.64	0.00151	CSO π–SC π^*
8c (C_{2h})	(+)425.39	1.76463	CSO π–CO π^*	383.37	0.00000	
8d (C_{2h})	(+)435.61	1.69794	CSO π–CO π^*	379.27	0.00000	
8e (C_s)	(+)430.85	1.71882	CSO π–CO π^*	(+)382.01	0.00005	CSO π–SC π^*
8f (C_s)	(+)433.31	1.58753	CSO π–CO π^*	(+)411.07	0.00152	CSO π–SC π^*
9a (C_s)	(+)396.01	1.15860	CS π–CO π^*	(+)370.70	0.00067	CN π–CO π^*
Thiophene	358.47	0.00000		(−)285.20	0.01684	SC π–CS π^*
Indole	(+)281.06	0.01065	N π–C π^*	(−)249.18	0.26964	C π–C π^*
L-Tryptophan	(+)290.54	0.00252	π–π^*–COO^-	(+)288.86	0.01214	N π–C π^*

Dip. len. = dipole length

Considerably more time-consuming CI-S calculations were required for accuracy within 45 nm. A CI-S/aug-cc-pCVDZ calculation on thiophene took 44 CPU minutes (41 nm error), and the SEA//STO-6G(d,p) calculation took 3 CPU seconds (3 nm error), on a Pentium 4M 3.056 GHz system. On the same system, diheptylindophenine runs using the 11 highest occupied and 11 lowest unoccupied molecular orbitals took 20 CPU seconds each.

Diheptylindophenines and indophenines **8a–8f** and **i8a–i8f** were found to be blue because of absorptions from electronic transitions between spatially congruent π and π^* molecular orbitals delocalized across carbon, nitrogen, oxygen, and sulfur atomic orbitals. The effects of conjugated thiophene moieties replacing the isatin moiety β-carbonyls in **8a–8f** and **9a** move these absorptions to the blue relative to their locations in *n*-heptylisatin, and the diheptyl groups in **8a–8f** move these absorptions slightly to the red relative to **i8a–i8f** and isatin.

Acknowledgments Some computer time and funding was provided by my employer at the beginning of this research, the Virginia Commonwealth University (VCU) Department of Academic Technology (SGI O2, SGI Origin 200, SGI Origin 2000), and by the VCU Center for the Study of Biological Complexity (64 CPU Beowulf cluster). Computer time was also supplied by Dr. Daniel P. Cook at the VCU Department of Mechanical Engineering (now at the University of Nevada, Las Vegas; SGI Power Challenge XL, two SGI Origin 2000's), and the late Dr. Bijan K. Rao at the VCU Department of Physics (SGI Origin 300). Several years ago Dr. Glenn E. Kellogg at the Medical College of Virginia's Department of Medicinal Chemistry provided access to Sybyl as part of research studying indole, phenyl, and naphthalene moiety compounds in biological systems. A few of the geometry optimized structures created for that study were used as starting points for some of the molecules studied here.

References

1. Baeyer A (1879) Untersuchungen über die Gruppe des Indigblaus. Berl Dtsch Chem Ges 12:1309–1319
2. Moore GE (1879) Report on the progress of analytical chemistry. J Am Chem Soc 1:527–587
3. Meyer V (1882) Ueber Benzole verschiedenen Ursprungs. Berl Dtsch Chem Ges 15:2893–2894
4. Meyer V (1883) Ueber den Begleiter des Benzols im Steinkohlentheer. Berl Dtsch Chem Ges 16:1465–1478
5. Meyer V (1883) Untersuchungen über die Thiophengruppe. Berl Dtsch Chem Ges 16:2172–2176
6. Meyer V (1888) Die thiophengruppe. Druck und Verlag Friedrich Vieweg und sohn, Braunschweig
7. Schlenk W, Blum O (1923) Über die konstitution des indophenins. Liebigs Ann Chem 433:95–103
8. Heller GZ (1924) Zur konstitution des indophenins. Angew Chem 52:1017–1018
9. Ray FE (1941) Organic chemistry. JP Lippincott, Chicago, p 627
10. Ballantine JA, Fenwick RG (1970) A reinvestigation of the structure of indophenine. Some new evidence. J Chem Soc C 14:2264–2266
11. Tormos GV, Belmore KA, Cava MP (1993) The indophenine reaction revisited. Properties of a soluble dialkyl derivative. J Am Chem Soc 115:11512–11515
12. Glossman-Mitnik D (2007) CHIH-DFT determination of the molecular structure and infrared and ultraviolet spectra of azathiophenes. Theor Chem Acc 117:57–68
13. Nåkansson R, Nordén B, Thulstrup EW (1977) Magnetic circular dichroism of heterocycles: thiophene. Chem Phys Lett 50:306–308
14. Nordén B, Nåkansson R, Pedersen PB, Thulstrup EW (1978) The magnetic circular dichroism of five membered ring heterocycles. Chem Phys 33:355–366
15. Kossmehl G, Manecke G (1968) Über die synthese polymerer indophenine und deren elektrische eigenschaften. Makromol Chem 113:182–189
16. Martinez F, Naarmann H (1990) New oligomers with isatin. Condensation reactions of thiophene and 2,2'-bithiophene with isatin. Angew Makromol Chem 178:1–16
17. Albinsson B, Kubista M, Nordén B, Thulstrup EW (1989) Near-ultraviolet electronic transitions of the tryptophan chromophore: linear dichroism, fluorescence anisotropy, and magnetic circular dichroism spectra of some indole derivatives. J Phys Chem 93:6646–6654
18. Berden G, Meerts WL, Jalviste E (1995) Rotationally resolved ultraviolet spectroscopy of indole, indazole, and benzimidazole: Inertial axis reorientation in the $S_1(^1L_b) \leftarrow S_0$ transitions. J Chem Phys 103:9596–9606

19. Park H, Lee S, Hagberg DP, Marinado T, Karlsson KM, Nonomura K, Qin P, Bochloo P, Brinck T, Hagfeldt A, Sun L (2007) Tuning the HOMO and LUMO energy levels of organic chromophores for dye sensitized solar cells. J Org Chem 72:9550–9556
20. Sobolewski AL, Domcke W (1999) Ab initio investigations on the photophysics of indole. Chem Phys Lett 315:293–298
21. Wan J, Meller J, Hada M, Ehara M, Nakatsuji H (2000) Electronic excitation spectra of furan and pyrrole: Revisited by the symmetry adapted cluster-configuration interaction method. J Chem Phys 113:7853–7866
22. Ramakrishna G, Bhaskar A, Bauerle P, Goodson III T (2008) Oligothiophene dendrimers as new building blocks for optical applications. J Phys Chem A 112:2018–2026
23. da Silva JFM, Garden SJ, Pinto AC (2001) The chemistry of isatins: a review from 1975 to 1999. J Braz Chem Soc 12:273–324
24. Tretiak S, Mukamel S (2002) Density matrix analysis and simulation of electronic excitations in conjugated and aggregated molecules. Chem Rev 102:3171–3212
25. Casado J, Miller JJ, Mann KR, Pappenfus TM, Hernández V, López Navarrete JT (2002) Experimental and theoretical study of the infrared and Raman spectra of a substituted sexithiophene in five oxidation states. J Phys Chem B 106:3597–3605
26. Can M, Özaslan H, Pekmez NÖ, Yildiz A (2003) Chemical synthesis of thiophene–pyrrole copolymer. Acta Chim Slov 50: 741–750
27. Stephens PJ (1970) Theory of magnetic circular dichroism. J Chem Phys 52:3489–3516
28. Stephens PJ (1974) Magnetic circular dichroism. Ann Rev Phys Chem 25:201–232
29. Wan J, Hada M, Ehara M, Nakatsuji H (2001) Electronic excitation spectrum of thiophene studied by symmetry-adapted cluster configuration interaction method. J Chem Phys 114:842–850
30. Hariharan PC, Pople JA (1973) The influence of polarization functions on molecular orbital hydrogenation energies. Theor Chim Acta 28:213–222
31. Francl MM, Pietro WJ, Hehre WJ, Binkley JS, Gordon MS, DeFrees DJ, Pople JA (1982) Self-consistent molecular orbital methods. XXIII. A polarization-type basis set for second-row elements. J Chem Phys 77:3654–3665
32. Shillady DD, Castevens CM, Trindle C, Sulik J, Klonowski P (2003) Conformational complexity of melatonin in water and methanol. Biophys Chem 105:471–494
33. SYBYL 6.8, Tripos Inc., 1699 S Hanley RD, St. Louis
34. Schmidt MW, Baldridge KK, Boatz JA, Elbert ST, Gordon MS, Jensen JH, Koseki S, Matsunaga N, Nguyen KA, Su SJ, Windus TL, Dupuis M, Montgomery JA (1993) General atomic and molecular electronic structure system. J Comput Chem 14: 1347–1363
35. Gordon MS, Schmidt MW (2005) Advances in electronic structure theory: GAMESS a decade later. In: Dykstra CE, Frenking G, Kim KS, Scuseria GE (eds) Theory and applications of computational chemistry, the first forty years. Elsevier, Amsterdam
36. Shillady DD, Billingsley FP, Bloor JE (1971) Valence shell calculations on polyatomic molecules IV. The effect of deorthogonalization on CNDO/2 dipole moments and charge distributions. Theor Chim Acta 21:1–8
37. Sprinkel FM, Shillady DD, Strickland RW (1975) MCD studies of indole, DL-tryptophan and serotonin. J Am Chem Soc 97:6653–6657
38. Foresman JB, Head-Gordon M, Pople JA, Frisch MJ (1992) Toward a systematic molecular orbital theory for excited states. J Phys Chem 96:135–149
39. Del Bene J, Jaffe HH (1968) Use of the CNDO method in spectroscopy. I. Benzene, pyridine, and the diazines. J Chem Phys 48:1807–1813
40. Takata S, Ono Y, Ueda Y (1985) Extension of the CNDO/S method to the calculation of aromatic and heterocyclic compounds containing Si, P, S and Cl. Chem Pharm Bull 33:3077–3091
41. Hug W, Wagnière G (1970) Molecular orbital calculations of rotational strengths: A study of skewed diketones. Theor Chim Acta 18:57–66
42. ArgusLab 4.0.1, Mark A. Thompson, Planaria Software LLC, Seattle, http://www.arguslab.com
43. Frisch MJ, Trucks GW, Schlegel HB, Scuseria GE, Robb MA, Cheeseman JR, Zakrzewski VG, Montgomery Jr., JA, Stratmann RE, Burant JC, Dapprich S, Millam JM, Daniels AD, Kudin KN, Strain MC, Farkas O, Tomasi J, Barone V, Cossi M, Cammi R, Mennucci B, Pomelli C, Adamo C, Clifford S, Ochterski J, Petersson GA, Ayala PY, Cui Q, Morokuma K, Rega N, Salvador P, Dannenberg JJ, Malick DK, Rabuck AD, Raghavachari K, Foresman JB, Cioslowski J, Ortiz JV, Baboul AG, Stefanov BB, Liu G, Liashenko A, Piskorz P, Komaromi I, Gomperts R, Martin RL, Fox DJ, Keith T, Al-Laham MA, Peng CY, Nanayakkara A, Challacombe M, Gill PMW, Johnson B, Chen W, Wong MW, Andres JL, Gonzalez C, Head-Gordon M, Replogle ES, Pople JA (2002) Gaussian 98, Revision A.11.3. Gaussian, Pittsburgh
44. Calzaferri G, Marcolli C (1995) Molecular geometries by the extended-Hückel molecular orbital method: A comment. J Phys Chem 99:3895–3897
45. Calzaferri G, Rytz R (1995) Electronic transition oscillator strength by the extended Hückel molecular orbital method. J Phys Chem 99:12141–12150
46. Rytz R, Glaus S, Brändle M, Brühwiler D, Calzaferri G (2000) ICON-EDiT 2000 manual, http://iacrs1.unibe.ch/program/iconedit.html
47. Calzaferri G, Fross L, Kamber I (1989) Molecular geometries by the extended Hückel molecular orbital method. J Phys Chem 93:5366–5371
48. Brändle M, Calzaferri G (1993) 166. Molecular geometries by the extended-Hückel molecular orbital method III: Band-structure calculations. Helv Chim Acta 76:924–951
49. Seifert R, Kunzmann A, Calzaferri G (1998) Die gelbe farbe von silberhaltigem Zeolith A. Angew Chem 110:1603–1606
50. Rytz R, Calzaferri G (1997) Electronic transition oscillator strengths in solids: an extended Hückel tight-binding approach. J Phys Chem B 101:5664–5674
51. Palmer MH, Walker IC, Guest MF (1999) The electronic states of thiophene studied by optical (VUV) absorption, near-threshold electron energy-loss (EEL) spectroscopy and ab initio multi-reference configuration interaction calculations. Chem Phys 241:275–296
52. Ohyama T, Mita H, Yamamoto Y (2005) Binding of 5,10,15,20-tetrakis (*N*–methylpyridinium-4-yl)-21H,23H-porphyrin to an AT-rich region of a duplex DNA. Biophys Chem 113:53–59
53. Prieto I, Pedrosa JM, Martín-Romero MT, Möbius D, Camacho L (2000) Characterization and structure of molecular aggregates of a tetracationic porphyrin in LB films with a lipid anchor. J Phys Chem B 104:9966–9972
54. Gouterman M (1961) Spectra of porphyrins. J Mol Spec 6:138–163
55. Gouterman M, Wagnière GH, Snyder LC (1963) Spectra of porphyrins—part II. Four orbital model. J Mol Spec 11:108–127
56. Susumu K, Maruyama H, Kobayashib H, Tanaka K (2001) Theoretical approach to the design of supramolecular conjugated porphyrin polymers. J Mater Chem 11:2262–2270
57. Spitler EL, Shirtcliff LD, Haley MH (2006) Systematic structure-property investigations and ion-sensing studies of pyridine-derivatized donor/acceptor tetrakis(arylethynyl)benzenes. J Org Chem 72:86–96
58. Zucchero AJ, Wilson JN, Bunz UHF (2006) Cruciforms as functional fluorophores: Response to protons and selected metal ions. J Am Chem Soc 128:11872–11881

59. Sørensen JK, Vestergaard M, Kadziola A, Kilså K, Nielsen MB (2006) Synthesis of oligo (phenyleneethynylene)-tetrathiafulvalene cruciforms for molecular electronics. Org Lett 8:1173–1176
60. Lopez X, Marques MAL, Castro A, Rubio A (2005) Optical absorption of the blue fluorescent protein: a first-principles study. J Am Chem Soc 127:12329–12337
61. Holmquist B, Vallee BL (1973) Tryptophan quantitation by magnetic circular dichroism in native and modified proteins. Biochemistry 12:4409–4417
62. McKee HC, Herndon K, Withrow JR (1948) Estimation of thiophene in gasoline. Anal Chem 20:301–303
63. Thompson CJ, Coleman HJ, Mikkelsen L, Yee D, Ward CC, Hall HT (1956) Identification of thiophene and 2-methyl thiophene in virgin petroleum. Anal Chem 28:1384–1387